Review of achievements and recording perspectives of rotational seismology

Anna T. Kurzych, Leszek R. Jaroszewicz
Institute of Applied Physics, Military University of Technology, 2 gen. S. Kaliskiego Str., Warsaw, Poland PL-00-908
Elproma Electronics Ltd., 2A Duńska Str.,Czosnów, Poland PL-05-152

ELPROMA

39th ESC2024

A view shows damage at an old mosque in the historic city of Marrakech, following a powerful earthquake in Morocco, September 9, 2023 [https://edition.cnn.com/2023/09/10/africa/mosque-earthquake-damage-marrakech-intl/index.html]

Building damanged by the February 2011 earthquake in Christchurch, New Zealand. [https://www.usgs.gov/media/images/earthquake-damaged-building]

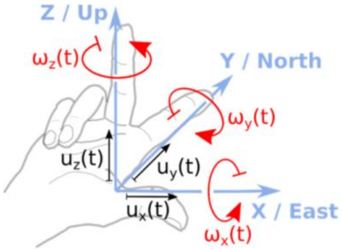

2006

The International Working Group on Rotational Seismology (IWGoRS, www.rotational-seismology.org) was initiated during a meeting organized by the United States Geological Survey in Menlo Park

ROTATIONAL SEISMOLOGY

2009

RS - a new, emerging field for the study of all aspects of rotational ground motion induced by earthquakes, explosions, and ambient vibrations [Lee et al. BSSA, 2009, 99, 945-957]

Seismological application

broadband seismology [Igel et al., Geophys. J. Int., 168(1), (2006), 182–197], strong-motion seismology [Anderson, 2003, Chap. 57, 937-965], earthquake physics [Teisseyre et al. Springer, 2006; Springer, 2008], seismic hazards [McGuire, Earthq. Eng. Struct. D., 37, (2008), 329–338], seismotectonics [www.geophysik.uni-uenchen.de/~igel/Lectures/Sedi/sedi_tectonics.ppt], geodesy [Carey, Expanding Earth Symposium, (1983), 365-372], physicists using Earth-based observatories for detecting gravitational waves [Ju et al., Rep. Prog. Phys., 63, (2000), 1317–1427; Lantz et al., BSSA, 99, (2009), 980-989]

Engineering application

seismic behaviour of irregular and complex civil structures [Trifunac, BSSA, 99, (2009), 968-97; Mustafa, InTech, 2015]

Seismological application

Energy generated during an earthquake propagates not only in a form of linear motions but also in rotational ones.

Earthquakes are undoubtedly one of the most complex phenomena and it is hard to entirely reflect their complexity in theoretical models

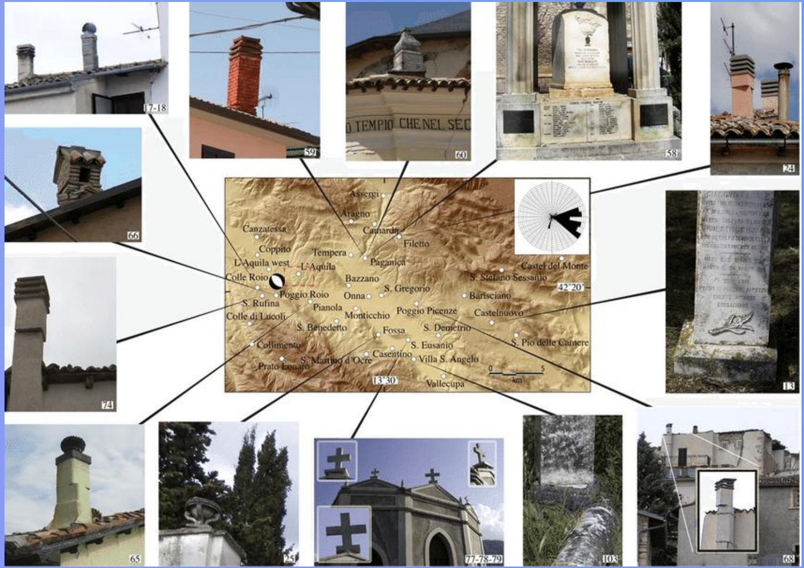

Map of the sites of observation of rotational effects and examples of rotationsafter 2009 L'Aquila earthquake [Cucci, L. & Tertulliani, A.. (2011), BSSA, 101, 1109-1120]

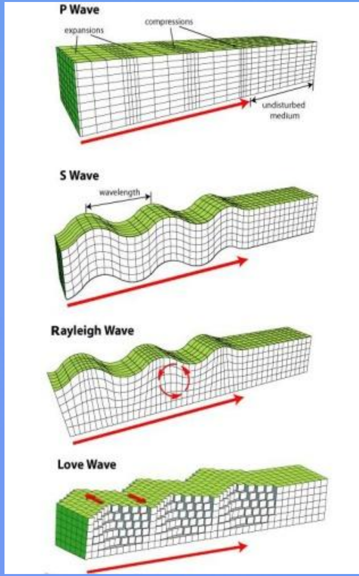

39th GENERAL ASSEMBLY OF THE EUROPEAN SEISMOLOGICAL COMMISSION
ESC2024
22-27 September 2024
CORFU, GREECE

Engineering application

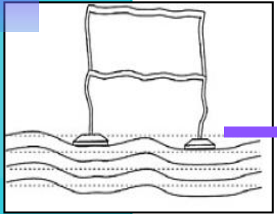

High frequency content

- **Local vibration of beams and columns**
- Meaningless motion of the building center of mass

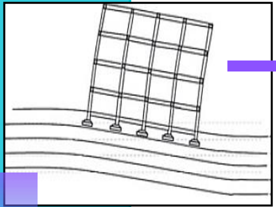

Low frequency content

- Higher stress in structural element
- **Overturning moment**
- Horizontal displacement of the center of mass

[Castellani, Guidotti, 2nd Workshop of IWGoRS Masaryk ’s College Prague, (2010)]

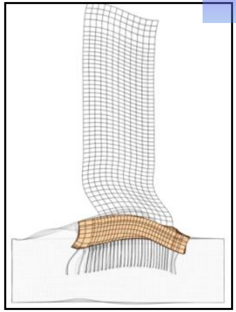

Snapshot of the model of displacement response to an incident plane P-wave half sine displacement pulse with 45° incident angle (view from South)

[Todorovska M. I., WCEE2024 Processing, 2024]

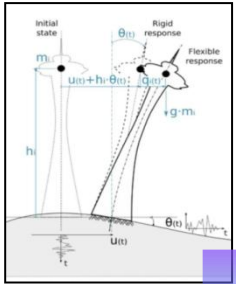

A slender structure under horizontal-rocking ground vibrations [Bońkowski et al., Engineering Structures 155, 387–393, 2018]

Classification of rotation measurements

Strong-motion of the order of tens of µrad/s and more	Rotation with a very low amplitude of the order of tens of 10^{-7} rad/s or less
• Rotational motions of the ground in the near-source field • Rotation associated with volcanic eruptions • Rotation recorded during chemical explosions • Rotation connected with engineering seismology	• Rotation measurements of teleseismic waves • Measurements of rotation related to the physics of seismological interactions • Rotation studies in a micromorphic medium

The frequency range can reach 10^{-4} Hz to 100 Hz;

Indirect rotation research by numerical conversion

	Ref.	Freq. [Hz]	ES	M_w	R [km]	PGV_h [m/s]	PGV_v [m/s]	$PG\omega_z$* [µrad]	$PG\omega_z$ [mrad/s]	$PG\omega_x$* [µrad]	$PG\omega_x$ [mrad/s]	$PG\omega_y$* [µrad]	$PG\omega_y$ [mrad/s]
1982	Bouchon & Aki		strike-slip fault	6.6	1	1/1.6	-	200/ 300	1.2/1.5	700	-		
2003	Huang	<1.0	The 1999 Chi-Chi, Taiwan earthquake (thrust fault)	7.6	6	0.33	0.50	171	0.385	44	0.126	177	0.331
2008	Spudich & Fletcher	< 3.6	2004 Parkfield, California, earthquake and aftershocks (strike-slip fault)	6.0	8.8	0.25	-	88.1	1.09	68.9	0.925	-	-
				4.7	14.0	0.012		4.69	0.0944	4.74	0.0926		
				5.1	14.4	0.060		20	0.446	0.177	0.372		
				4.9	18.3	0.027		13.6	0.247	9.73	0.215		
2009	Stupazzini, et al.	< 2	valley of Grenoble, French (strike-slip)	6.0	0.02 - 0.90	3315	-	1 690	8.24	1.31	8.66	-	-
2009	Wang, et al.	<0.5	Newport–Inglewood strike-slip	7.0	<80	-	-	-	3.00*		0.350*	-	0.6*
2019	Cao & Mavroeidis		hypothetical strike-slip earthquake	6 6.4 7.2 7.6	1-50	<0.72	<0.24	69.2-194.2		16.9-94.3	-	22.7-98.5	-
			dip-slip earthquake	6 6.4 6.8 7.2 7.6	1-50	<0.66	<0.93	54.1-144.3		117.9 -421.9	-	144.2-325.3	-
2021	Cao & Mavroeidis	< 1.0	Izmit earthquake 1999	7.5	1-50	0.11-0.63*	0.03-0.19*	52.6-155*	-	6.2-43.3*	-	10.7-47.4*	-
			2004 Parkfield	6.0	1-50	0.005-0.23*	0.003-0.045*	5.6-35.5*		2.5-23.1*		1.4-30.7*	
			1979 Imperial Valley	6.5	1-50	0.06-0.83*	0.007-0.13*	21-178*		9.7-89*		3.9-29.8*	

Bouchon and Aki used the discrete wavenumber representation method

Huang presented calculated rotations from translational velocities by numerically integrating accelerograms from a dense acceleration system

Spudich & Fletcher provides an estimate of the rotation of the September 28, 2004, mainshock in Parkfield, California

Stupazzini et al. simulated the rotational wave field 3D numerical modeling

Wang et al. simulated using a finite-difference method over a frequency range of up to 0.5 Hz. The analysis showed that the variability of the hypocenter leads to significant changes in the ground rotation speed.

Cao and Mavroeidis finite differential translational motions generated at very closely spaced stations

Parameters of the rotation (selected maximum value) obtained indirectly by numerical analysis. Legend: Y – year of publication, Ref. – reference, ES – earthquake source mechanism, M_w - magnitude, R – epicentral distance, PGV_h – peak value of horizontal ground velocity, PGV_v – peak value of vertical ground velocity, $PG\omega_{z,x,y}$ – peak value of rotational velocity around the particular axis.

* $PG_{\omega z,x,y}$ – ground rotation around the particular axis depending on the distance

Rotation effects recordings during natural earthquakes

Y	Ref.	ES	Sensor	M_w	R [km]	PGV_h [mm/s]	PGV_v [mm/s]	$PG\omega_z$ [mrad/s]	$PG\omega_x$ [mrad/s]	$PG\omega_y$ [mrad/s]
1998, 2006	Takeo	strike-slip fault, 1997	Systron Donner triaxial gyro sensor	5.7	3.3	290	500	3.3	26	5.9
				5.3	3.3	200	100	8.1	27	30
2009	Takeo	seismic swarm activities at offshore Ito, Japan, 1998	Systron Donner triaxial gyro sensor	5.0	5.6	100	60	3	6	8
				3.6	5.9	6	2	0.2	1	1
				2.4	4.9	6	0.3	0.03	0.2	0.2
2009	Liu *et al.*	local earthquakes at the HGSD station in eastern Taiwan	R-1	5.1	51	-	-	0.63	~0.4	~0.3
				2.5-6.63	14.3–260.4	-	-	0.004-0.63	-	-
2010	Brokešová & Málek	earthquake swarm in Western Bohemia, 2008	Rotaphone 3DOF	2.2	4.4	400	-	0.15	-	-
2013	Brokešová & Málek	an earthquake recorded at the station Sergoula, Greece	6 DOF Rotaphone	4.3	5	4.5	9	~0.4	~0.8	~0.7
2016	Yin *et al.*	215 events at The Garner Valley Downhole Array is in California, 2008-2014	R-1	3.0-7.2	14-207	-	-	0.006-0.453	-	0.004-0.7
2017	Jaroszewicz *et al.*	local earthquake, Jarocin, Poland	TAPS	3.8	200	-	-	0.005	-	-
			AFORS					0.039		
2018	Ringler *et al.*	local earthquake	Two SMHD (ATA)	4.2	0.5	22.1	11	1.12/0.85	-	2.11/1.86
		local earthquake		2.8	≤220	-	-	~0.0005	~0.00025	~0.00025
		155 local earthquake		≥ 2.0	≤220			0.0002–2	0.0002–2	0.0002–2
2020	Wassermann *et al.*	volcano-tectonic earthquake	BlueSeis-3A	5.3	1.5	2	1	2.4	2.5	2.4
2022	Wassermann *et al.*	Stromboli volcano, Italy activity	BlueSeis-3A	-	-	<0.01	<0.02	<0.0005	<0.001	<0.001

Parameters of the rotation recordings generated by natural earthquakes. Legend: Y – the year of publication, Ref. – reference, ES – earthquake source, M_w - magnitude, R – epicentral distance, PGV_h – peak value of horizontal ground velocity, PGV_v – peak value of vertical ground velocity, $PG\omega_{z,x,y}$ - peak value of rotational velocity about a particular axis

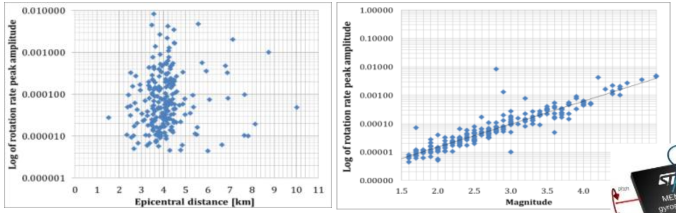

Takeo – 3-axial Gyro (Systron Donner)

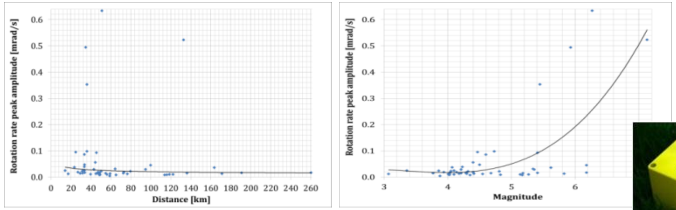

Liu, Yin – R-1 (Eentec)

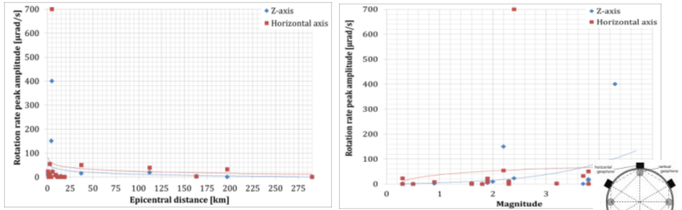

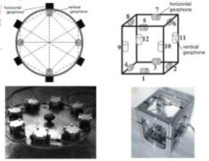

Brokesova – 3DOF, 6DOF Rotaphone (Czech Republic)

Teleseismic waves recordings

Y	Ref.	ES	Sensor	M_w	R [km]	PGV_h [m/s]	$PG\omega_z$ [nrad/s]	$PG\omega_x$ [nrad/s]	$PG\omega_y$ [nrad/s]
2000	Pancha et al.	New Ireland earthquake, 1999	C-II, G0	7.0	~4 700	-	10 (C-II)	5 (G0)	-
		Vanuatu earthquake, 1999	C-II	7.3	~3 500		8	-	
2005	Igel et al.	Thrust earthquake Japan	G-ring	8.1	~8 830		~35		
2007	Igel et al.	from local event, Germany to Great Andaman earthquake	G-ring	5-9	370–12 700	-	~0.10 –40	-	-
2009	Schreiber et al.	Earthquake Kamachatka, 2006	GEOsensor	7.6	~6 500	5 197	~10	-	-
		Earthquake Mexico, 2006		5.4	~2 000	4 646	~5		
		Earthquake California, 2007		3.6	~200	8 670	~16		
		Earthquake California, 2007		3.9	~250	14 512	~30		
2011	Lin et al.	Earthquake in Wenchuan Sichuan, China	R-1	7.9	1 948	<0.01	-	10 000	10 000
2012	Belfi et al.	Earthquake in Japan, 2011	G-Pisa	9.0	-	-	~60	-	-
2017	Ross et al.	earthquake Papua New Guinea, 2016	beam rotation sensor BRS	7.9	-	~$150\cdot10^{-6}$	-		~30*
		earthquake Vanuatu, 2016		6.7		~$6\cdot10^{-6}$			~2*
		earthquake New Caledonia, 2016		7.2		~$40\cdot10^{-6}$			~10*
		earthquake north of Ascension Island, 2016		7.1		~$15\cdot10^{-6}$			~4.5*
		earthquake New Zealand, 2016		7.8		~$200\cdot10^{-6}$			~60*
		earthquake of Panguna, Papua New Guinea, 2017		7.9		~$150\cdot10^{-6}$			~30*
2018	Simonelli et al..	Series of earthquakes in Italy, 2016	GINGERino	3.5–5.9	38 -77	-	~600–17 000	-	-
2020	Sollberger et al.	Earthquake Gulf of Alaska, 2018	ROMY	7.9	-	-	~6	~8	~4
2021	Igel et al.	Papua New Guinea earthquake, 2019	ROMY	7.6	14 000	-	~8.5	~9	-
		Turkey earthquake, 2019		5.7	1 500		~5	~9	
		Austria earthquake, 2018		3.8	144		~18.9	~18	

- strong earthquakes
- extremly distance R
- extremely low PGω (nrad/s) amplitude

GINGERino

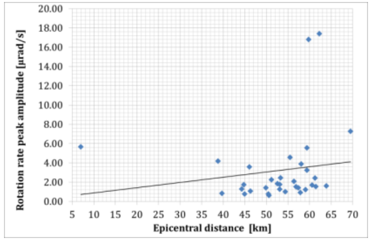

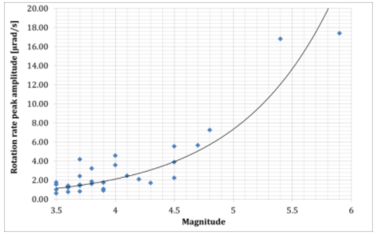

Requirements

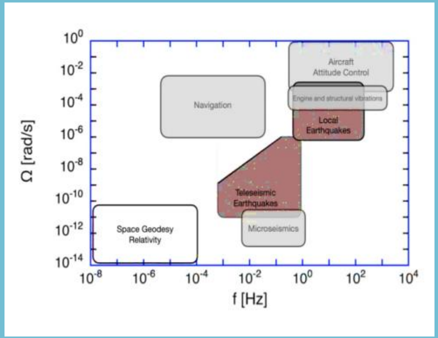

[Schreiber U, Kodet J, WCEE Processing, Milan, Italy 2024]

Engineering application

signal amplitude: up to 10 rad/s,
frequency: 0.01 Hz – 100 Hz

Seismological application

signal amplitude: from 10^{-7} rad/s,
frequency: 0.01 Hz – 0.1 Hz

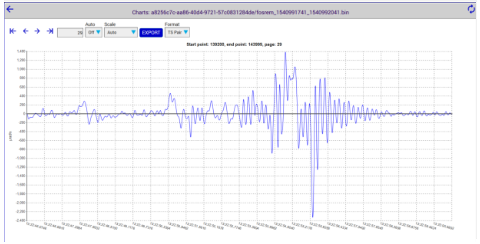

- Insensitivity to linear motion
- Mobility, stability with respect to environmental conditions, including changes of temperature
- Independent power supply
- Dynamic range 10^{-8} - 10 rad/s
- Frequency band 0.01 - 100 Hz
- Power consumption 5 – 8 W
- Thermal stability <0,1% / oC
- Calibration – in situ (permanently)

ROTATIONAL SEISMOGRAPH
network of seismometers + precise time source + recording device + network

Device	3-axial GYRO	TAPS	3DOF	6DOF	D	CY	R-1	AFORS-1	BlueSeis-3A
							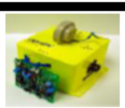		
Year of construction	2008	1998	2010	2012	2015	2019	2006	2010	2015
Sensitivity [nrad/s]	no data	100	16.7	2.16	3.77	0.042	1200	4	20
$\Omega_{Max.}$ [mrad/s]	873	100	10	287	31.7	31.68	0.1	64.3	0.1
Dynamic range [dB]	no data	120	100	120	120	120	110	124	135
Frequency range [Hz]	DC - 75	0.7 – 50	1 – 100	2 – 60	2 – 80	1–100	0.05 - 20	0.83-106	DC - 100
Sampling rate	no data	100	250	250	250	250	N/A	212	up to 200
Sensors: [No. x type]	MEMS	2 x SM-3	8 x LF-24	9; 12 SM-6	16 x SM-6	12 x SM-6	fluid MET	optical	optical
Eigen frequency	no data	45	1	4.5	4.5	4.5	N/A	N/A	N/A
Spacing of sensors [m]	N/A	0.28	0.3	0.3	0.4	0.3	N/A	N/A	N/A
Operating temp. [°C]	< 125	-10 – +45	-20 – +40	-20 – +40	-20 – +100	-40 – +70	-15 – +55	-10 – +50	-10 – +50
Weight [kg]	0.3	15	4.5	9.5	15.3	22	1.0	18	20
Dimensions [LxWxH] [cm]	no data	45x18x35	25* x 1	35x30x43	44.5x12	55*x50	12x12x9	70* x 16	30*x60

* diameter

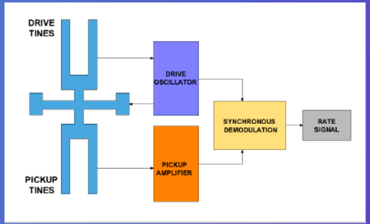

MEMS - vibrating tuning fork, vibrating-wheel, resonant wheel, hemispherical resonant, Foucault pendulum apply the Coriolis force to detect the angular velocity

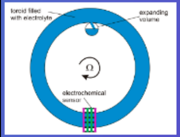

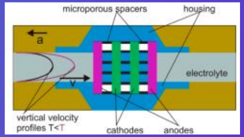

R-1 (R-2) - no flat above 1 Hz, 80 dB instead declare 110 dB, 27% (R-1) and 18% (R-2) signal deviation in temp. +20 - +50 C.

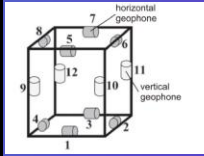

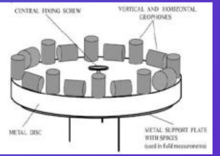

Rotaphone (3DOF, 6DOF, D) Ω is determined by more accurately as result of more than one geophone pair; frequency ranges are still too narrow

AFORS-1 (uniaxial), BlueSiei-3A (triaxial) optical system based on (or uses) FOG – physically the Sagnac effect in fiber-optic loop interferometer, mass-free (non-inertial) system -> probably the best solution for rotational seismograph fulfill all RS requirements.

BACKGROUND

The direct utilization of the Sagnac effect

Sagnac effect shows the difference between phase of two beams propagating around closed optical path, in opposite direction when this path is rotating with rotational rate Ω. In a fiber-optic implementation the rotation rate Ω is expressed by induced phase shift Δφ as:

$$\Omega = S_o \cdot \Delta\varphi = \frac{\lambda c}{4\pi RL} \cdot \Delta\varphi$$

L – length of the fiber in the sensor loop,
R – sensor loop radius,
λ – wavelength of used source,
c – velocity of the light in vacuum,
S_0 – the optical constant of interferometer

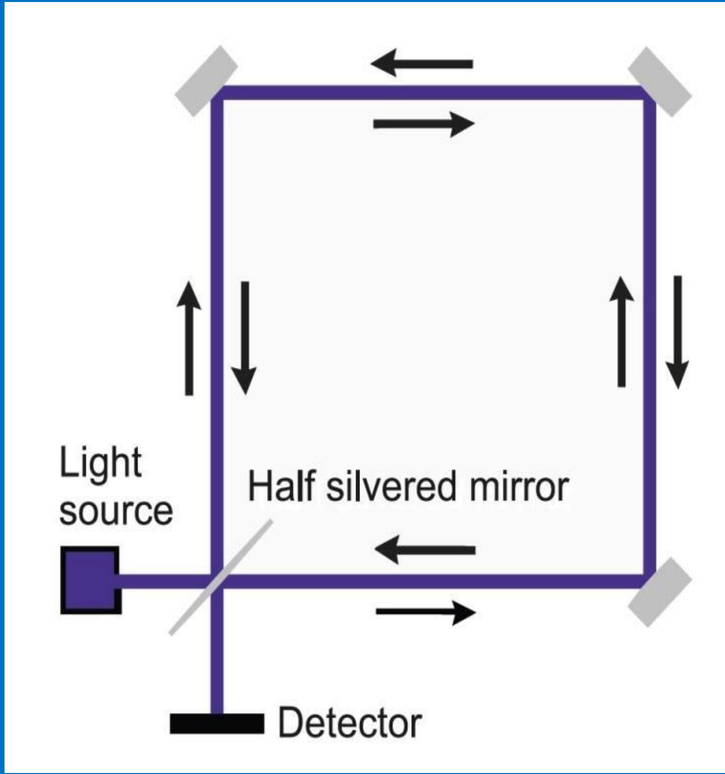

Fibre-Optic Seismograph

OPTICAL PART

generates the phase shift $\Delta\varphi$ proportional to the measured rotation rate Ω which is perpendicular to the sensor loop plane

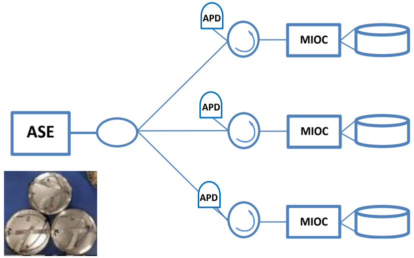

ELECTRONIC PART

enables to calculate and record information about rotational motions via digital closed-loop signal processing

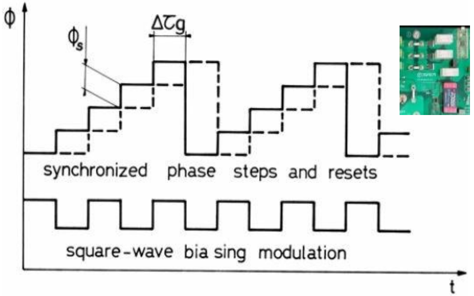

Laboratory analysis of FORS' parameters

Allan Variance analysis

Theoretically

$$ARW = \frac{\sqrt{2}\lambda c}{2\pi DL}\sqrt{\frac{4kT}{R\eta^2 P^2} + \frac{ei_d}{\eta^2 P^2} + \frac{e}{\eta P} + \frac{\lambda^2}{4c\Delta\lambda}}$$

where: λ – central light wavelength (1 550 nm), c – speed of light, D – loop diameter (0.25 m), L – loop length (about 6 000 m), k – Boltzmann's constant, T – temperature (293 K), R – resistance of the trans-impedance transducer of the photodetector device (20 kΩ), η – efficiency ratio of the photodiode (0.85 A/W), P – incident optical power on the APD, e – elementary charge, i_d – photodiode dark current (80 nA), $\Delta\lambda$ – spectral width of the light source (40 nm).

The calculated theoretical values of ARW for each optical head for four FORS type FOS6 were in the range of **4.49-4.85 nrad/√s**, depending on total optical losses and fiber length in the given optical head.

Allan Variance analysis

Data gathered in the Military University of Technology, Poland

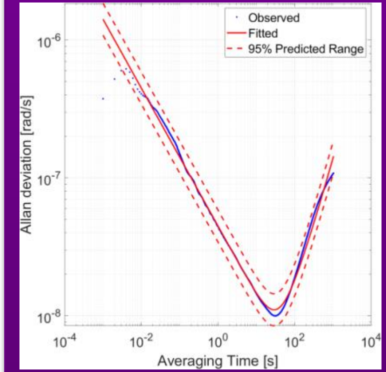

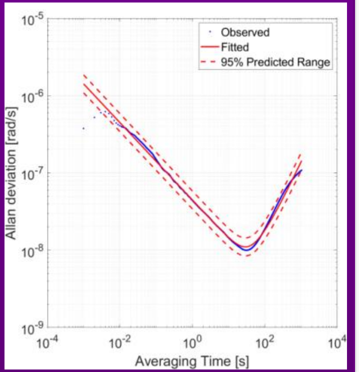

FOS6-01: ARW: 35 nrad/√s, BI: 10.0 nrad/s
FOS6-02: ARW: 45 nrad/√s, BI: 51.0 nrad/s

FOSREM as FOS remote controls by webpage

System control

Paramters change

Data downloading

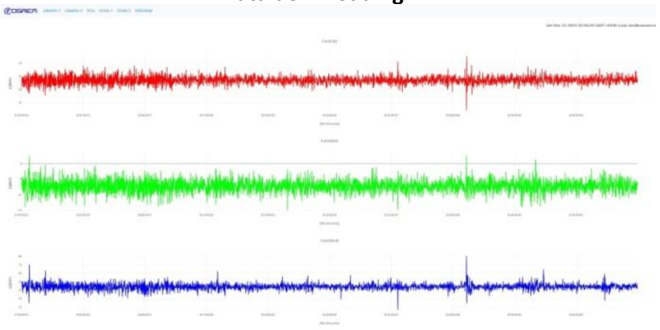

Localization

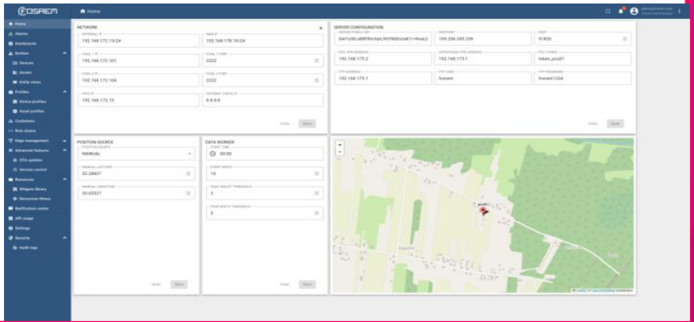

Correlation verification

FOS6-01 and FOS6-02 in the MUT laboratory on the rotary table

Field test in the Kampinos Nature Park by a pair of FORSs (FOS6-01 and FOS6-04)

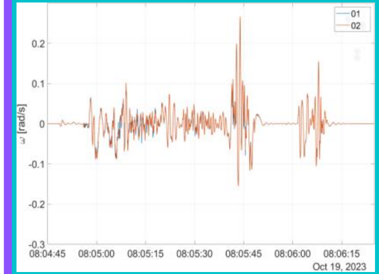

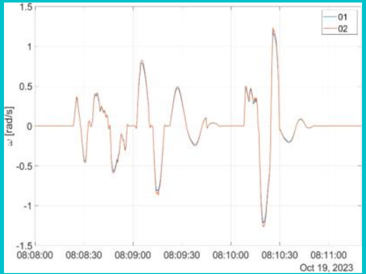

Signals recorded by FORSs Z-axes during the medium high-amplitude at a level of 0.25 rad/s and fast-changing excitations (at a level of 100 Hz) as well as high-amplitude at a level of 1.2 rad/s amplitude excitations

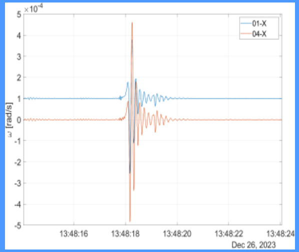

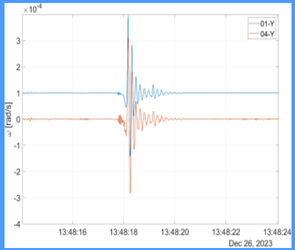

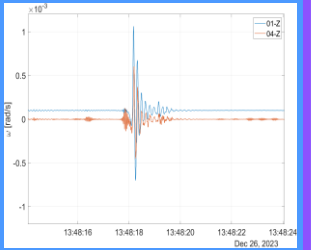

A weak recording (with an amplitude of about 0.5 mrad/s) generated by the wild animal (elk) moving in the field close to the FORSs location

Pearson correlation coefficient equal to 99.42% and 99.99 %

Pearson correlation of about 95% for the X axis, about 99% for Y axis, and about 99% for the Z axis

Rotation Detection During Detonation of an Explosive Charge

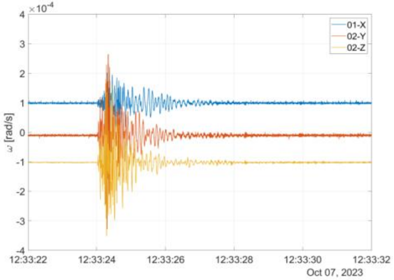

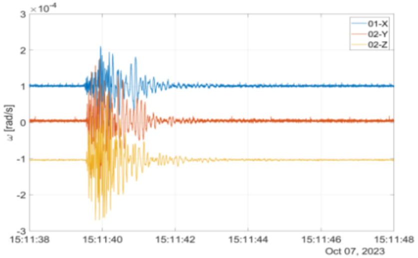

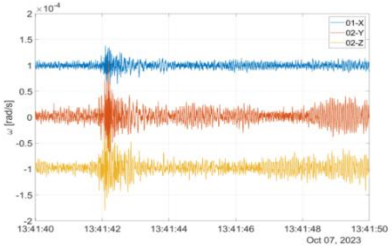

On the 7th of October 2023 there were three explosions performed:

1. 12:33 UTC, 5 kg of explosive, 3 m below the ground surface with surface discharge.
2. 13:41 UTC, 5 kg of explosive, 4.5 m below the ground surface without surface discharge.
3. 15:11 UTC, two 5 kg explosive charges installed 5 meters apart were detonated one after the other, 4.5 m below the ground surface, with a distance of 5 m between loads.

	A_{max} [µrad/s]			E_f [µrad]		
Explosion number/ Axis of FORS	X	Y	Z	X	Y	Z
Explosion 1	140	327	281	69	163	104
Explosion 2	38	108	83	41	98	94
Explosion 3	119	177	170	65	111	106

Conclusions

1 Data confirmed high reliability of recordings gathered by 3-axial Fibre-Optic Rotational Seismograph (correlation coefficient was near the value of 100%)

2 FORS recorded successfully artificial explosions in field test carried out in Szopowe, Poland which confirmed its usefulness of monitoring detonation tests, especially in border areas.

3 FORS main paramters:

- dynamics of 180 dB
- frequency detection bandpass: from 0.01 to 100 Hz
- built-in time scale synchronization system
  (accuracy 100ns)
- weight: less than 10 kg
- web-Based Management Interface
- possibility of mobile, autonomous operation

4 **Rotational seismology** undergoes a rapid development.
Future plans – 6 DoF recordings

Any questions?

You can find me at:

anna.kurzych@wat.edu.pl

a.kurzych@elpromaelectronics.com

https://fosrem.eu/

Thank you very much for attention

FOSREM - FROM SKY ACROSS GROUND UP TO UNDERGROUND

National Centre for Research and Development project POIR.01.01.01-00-1553/20-00

FOM-MEM - FIBRE-OPTIC MATRIX FOR MECHANICAL EVENTS MAPPING

Polish Agency for Enterprise Development project FENG.01.01-IP.02-1714/23